European Journal of Immunology

Innate immunity

Basic

Research Article

Differential sensitivity of inflammatory macrophages and alternatively activated macrophages to ferroptosis

Federica Piattini[#1], *Mai Matsushita*[#1], *Jonathan Muri*[1], *Peter Bretscher*[1], *Xiaogang Feng*[2], *Stefan Freigang*[1], *Jesmond Dalli*[3], *Christoph Schneider*[2] and *Manfred Kopf*[1]

[1] Institute of Molecular Health Sciences, Department of Biology, ETH Zurich, Zurich, Switzerland
[2] Institute of Physiology, University of Zurich, Zurich, Switzerland
[3] William Harvey Research Institute, John Vane Science Centre, London

Acumulation of oxidized membrane lipids ultimately results in ferroptotic cell death, which can be prevented by the selenoenzyme glutathione peroxidase 4 (Gpx4). In vivo conditions promoting ferroptosis and susceptible cell types are still poorly defined. In this study, we analyzed the conditional deletion of Gpx4 in mice specifically in the myeloid cell lineages. Surprisingly, development and maintenance of LysM$^+$ macrophages and neutrophils, as well as CD11c$^+$ monocyte-derived macrophages and dendritic cells were unaffected in the absence of Gpx4. Gpx4-deficient macrophages mounted an unaltered proinflammatory cytokine response including IL-1β production following stimulation with TLR ligands and activation of several inflammasomes. Accordingly, Gpx4$^{fl/fl}$LysM-cre mice were protected from bacterial and protozoan infections. Despite having the capacity to differentiate to alternatively activated macrophages (AAM), these cells lacking Gpx4 triggered ferroptosis both in vitro and in vivo following IL-4 overexpression and nematode infection. Exposure to nitric oxide restored viability of Gpx4-deficient AAM, while inhibition of iNOS in proinflammatory macrophages had no effect. These data together suggest that activation cues of tissue macrophages determine sensitivity to lipid peroxidation and ferroptotic cell death.

Keywords: Alternatively activated macrophages · ferroptosis · inflammation · glutathione · glutathione peroxidase 4

Additional supporting information may be found online in the Supporting Information section at the end of the article.

Introduction

Myeloid cells play a major role in tissue homeostasis, inflammation, and pathogen clearance [1]. Macrophages are among the cells that are recruited rapidly to the site of infection to provide an early defense against external invasion [2]. Tissue-resident macrophages act as sentinels to maintain tissue homeostasis by clearing senescent cells, contributing to tissue remodeling and to repair after inflammation or injury [3]. Macrophages are remarkably plastic and are capable of swift differentiation in response to environmental stimuli. Activation of TLRs, in combination with Th1 cytokines, such as IFN-γ, induces a proinflammatory macrophage phenotype [4]. These macrophages eliminate pathogens by phagocytosis, produce nitric oxide (NO) by

Correspondence: Prof. Manfred Kopf
e-mail: Manfred.Kopf@ethz.ch

[#]Federica Piattini and Mai Matsushita contributed equally to this work.

expression of iNOS, and release proinflammatory cytokines. Th2 cytokines, IL-4 and IL-13, stimulate generation of alternatively activated macrophage (AAM, also called M2) differentiation in response to parasitic infection or during the resolution phase of an inflammation, to promote tissue repair and homeostasis [3].

Oxidative burst is a vital effector mechanism deployed by myeloid cells for host defense. This process involves assembly of NADPH oxidase complex on phagosomal membranes, which readily catalyzes the reduction of molecular oxygen to superoxide, thereby generating ROS [5]. ROS at moderate concentrations act as signaling molecules that modulate proliferation, differentiation, and survival [6, 7]. However, at high concentrations, they are implicated in the pathogenesis of complex diseases, including progression of diabetes, neurodegenerative disease, and cancer [8–10]. Therefore, an intricate network of antioxidant defense systems helps neutralizing excessive ROS [11]. Antioxidant glutathione peroxidase 4 (Gpx4) is a unique intracellular lipid peroxidation-detoxifying enzyme that is vital for survival, as homozygous Gpx4-deficient mice die at the embryonic stage [12, 13]. Inactivation of Gpx4 detrimentally impacts homeostasis and pathophysiology, and is implicated in the progression of various programmed cell death pathways including apoptosis [14], necroptosis [15], ferroptosis [16–18], and pyroptosis [19]. Previously, we reported that T cells, B1 and marginal zone B cells require Gpx4 for homeostatic integrity and protection from infection, and undergo lipid peroxidation-induced ferroptotic cell death in its absence [17, 18, 20]. Inactivation of Gpx4 is the main etiology of ferroptosis, which is triggered by the accumulation of iron-dependent lipid peroxidation [16]. Inhibition of the cystine/glutamate antiporter system X_c^- (*Slc7a11* or xCT) has been additionally proposed to induce ferroptosis as it depletes intracellular cysteine for glutathione synthesis [21]. While the precise mechanism of how lipid peroxidation triggers ferroptosis is not known, the requirement for acyl-CoA synthetase long-chain family member 4 (ACSL4) provided an insight into the possibility that anabolic metabolism of acyl-CoA for phospholipid and triacylglycerol synthesis may be the cause of this destructive lipid peroxidation [22].

In this study, we analyzed the conditional deletion of Gpx4 in mice specifically in the myeloid cell lineage. Here, we report that Gpx4 is dispensable for generation and homeostasis of all mature myeloid populations including tissue-resident macrophages in the spleen, BM, peritoneum, and lung. Gpx4-deficient macrophages are capable of proinflammatory function and efficient control of intracellular bacterial and protozoan infections. However, IL-4-driven infection or IL-4 overexpression resulted in ferroptosis-mediated cell death of AAM. Our data reveal the unique antioxidant control of Gpx4 in macrophage biology.

Results

Gpx4 is required to sustain cell survival in AAM

To examine the survival and function of macrophages lacking Gpx4 in vitro, we used $Gpx4^{fl/fl}Cre^{ERT2}$ mice, in which Cre is ubiquitously expressed under the control of the Rosa26 locus upon tamoxifen injection, and generated BM-derived macrophages (BMDMs) [17]. Resting macrophages (M0) were polarized to inflammatory macrophages or AAM with LPS/IFN-γ or IL-4, respectively. Gpx4 expression was abrogated in $Gpx4^{fl/fl}Cre^{ERT2}$ BMDMs treated with tamoxifen in vitro, indicating robust deletion of Gpx4 gene using the inducible system (Fig. 1A). Measuring the viability of in vitro activated BMDMs, we found that the number of live cells decreased after 24 h in M0 and IL-4-stimulated $Gpx4^{fl/fl}Cre^{ERT2}$ BMDMs (Fig. 1B and C). In support of this finding, the absence of Gpx4 resulted in increased frequencies of dead cells, quantified by eFluor780 viability dye, in M0 and IL-4, but not in LPS/IFN-γ polarized BMDMs (Fig. 1D). Similar results were obtained comparing BMDM from $Gpx4^{fl/fl}LysM^{cre}$ and littermate controls (Supporting information Fig. S1A-C). Furthermore, ferroptosis induction was independent of the presence of M-CSF during stimulation (data not shown). Expression of iNOS, the prototype marker of inflammatory macrophages, and NO production following simulation with TLR ligands together with IFN-γ were unaltered in Gpx4-deficient BMDM (Fig. 1E, Supporting information Fig. S1D). Surface protein levels of RELMα and CD301 (Fig. 1E) and expression of Arg1, Ym1, and Fizz1 genes, which are hallmarks of AAM, were similarly upregulated upon IL-4 stimulation (Fig. 1F, Supporting information Fig. S1E). Moreover, DNA replication, as evaluated by 5-ethynyl-2'–deoxyuridine (EdU) incorporation in IL-4 stimulated cells, was comparable to controls (Supporting information Fig. S1F). To further investigate the function of in vitro activated macrophages, we measured proinflammatory cytokine production by BMDMs upon stimulation with TLR ligands, including LPS (TLR4), unmethylated CpG containing DNA (CpG; TLR9), imiquimod (R837; TLR7), and yeast-derived zymosan (TLR2), and found an unaltered capacity to produce proinflammatory cytokines IL-6, IL-12, and TNF-α in the absence of Gpx4 (Fig 1G, Supporting information Fig. S1G). We also detected a comparable secretion of IL-1β upon NLRP3-, AIM2-, and NLRC4-mediated inflammasome activation in Gpx4-deficient and control BMDMs (Fig 1H, Supporting information Fig. S1H and I). Gpx4 is, therefore, crucial for the survival of M0 and AAM but is dispensable for proinflammatory macrophage survival, activation, and function.

Inflammatory macrophages are resistant to lipid peroxidation-driven ferroptosis in absence of *Gpx4*

As in vitro-activated Gpx4-deficient M0 and AAM displayed high mortality, we speculated that ROS accumulation, and thereby ferroptosis, might be induced in these cells. We tested this in $Gpx4^{fl/fl}Cre^{ERT2}$ BMDMs that exhibited low viability after 24 h under M0 and IL-4 conditions (Fig. 1C), and assessed the viability in the presence of ferroptosis inhibitor ferrostatin-1 (Fer-1). While Fer-1 had no effect on LPS/IFN-γ-treated BMDMs, M0 and IL-4-stimulated $Gpx4^{fl/fl}Cre^{ERT2}$ cells maintained similar numbers compared to controls and correspondingly displayed low percentages of dead cells in the presence of Fer-1 (Fig. 2A and B). We next

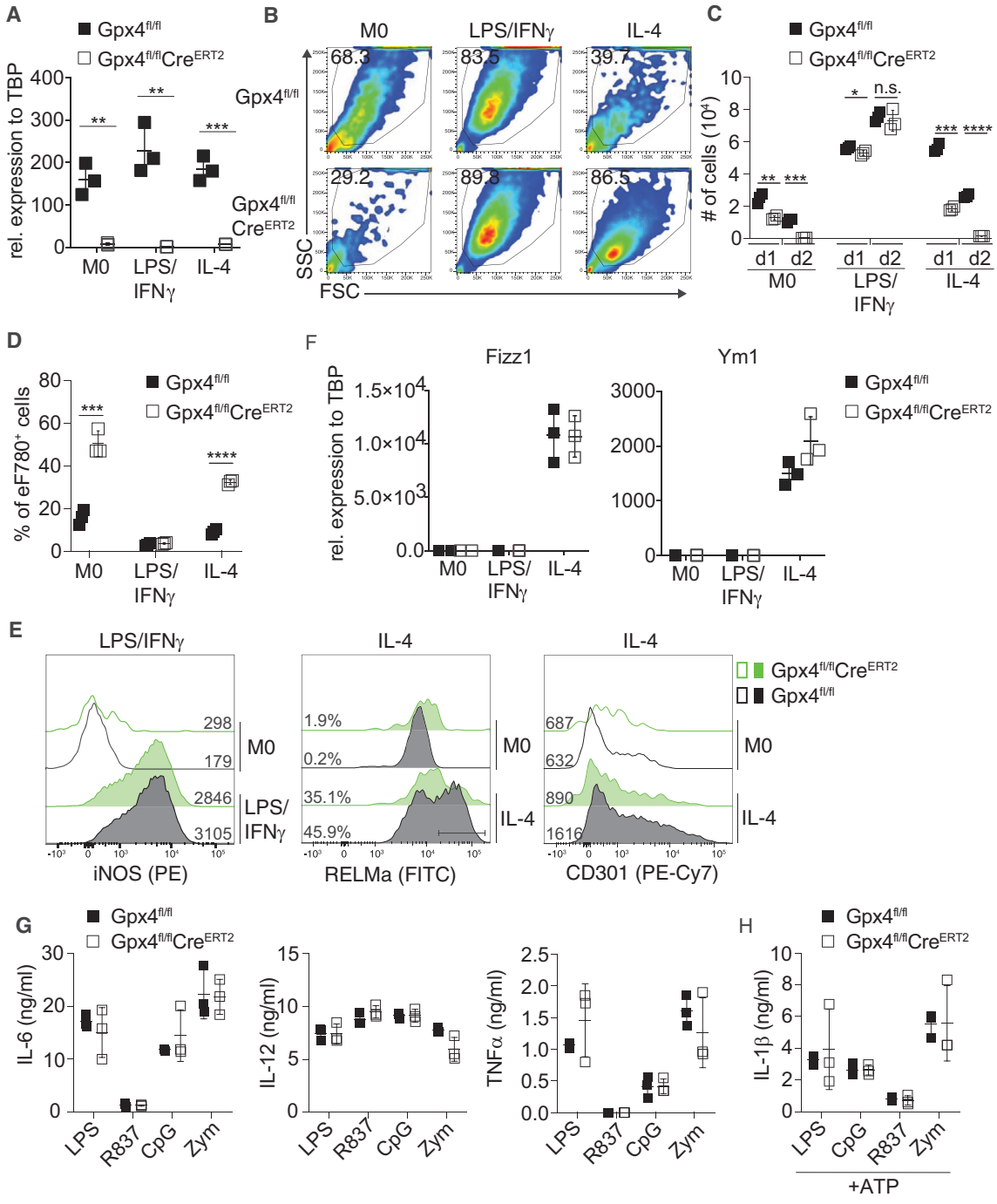

Figure 1. Gpx4-deficient BMDMs have a survival defect when differentiated to AAM. (A-F) BMDMs were unstimulated (M0) or stimulated with LPS (20 ng/mL) plus IFN-γ (50 ng/mL) or IL-4 (20 ng/mL) for up to 48 h. (A) Real-time RT-PCR analysis for Gpx4 expression relative to TATA-box binding protein (TBP), a housekeeping gene. (B) Representative flow cytometry plots of forward scatter (FSC) versus side scatter (SSC) after 48 h. (C) Quantification of absolute cell numbers at day 1 and 2 poststimulation. (D) Percentage of dead cells (eFluor780$^+$) after 48 h measured by flow cytometry. (E) Representative expression of iNOS, RELMα, and CD301 in M0 or after 48 h with LPS/IFN-γ or IL-4 assessed by flow cytometry. Numbers indicate MFI (iNOS and CD301) or frequency of positive cells (RELMα). (F) Real-time RT-PCR analysis for Fizz1, and Ym1 expressions relative to TBP after 24 h. (G) BMDMs were stimulated with LPS (100 ng/mL), CpG (100 nM), R837 (5 μg/mL), or Zymosan (Zym; 20 μg/mL) overnight. Cytokines from cultural supernatant were measured by ELISA. (H) BMDMs were stimulated as (G) with additional ATP (2 mM) for 2 h prior to cultural supernatant harvest. IL-1β was detected by ELISA. Error bars indicate mean ±SD. $^*p < 0.05$; $^{**}p < 0.01$; $^{***}p < 0.001$; $^{****}p < 0.0001$ (two-tailed Student's *t*-test). Data are representative of at least three independent experiments with three samples per experiment.

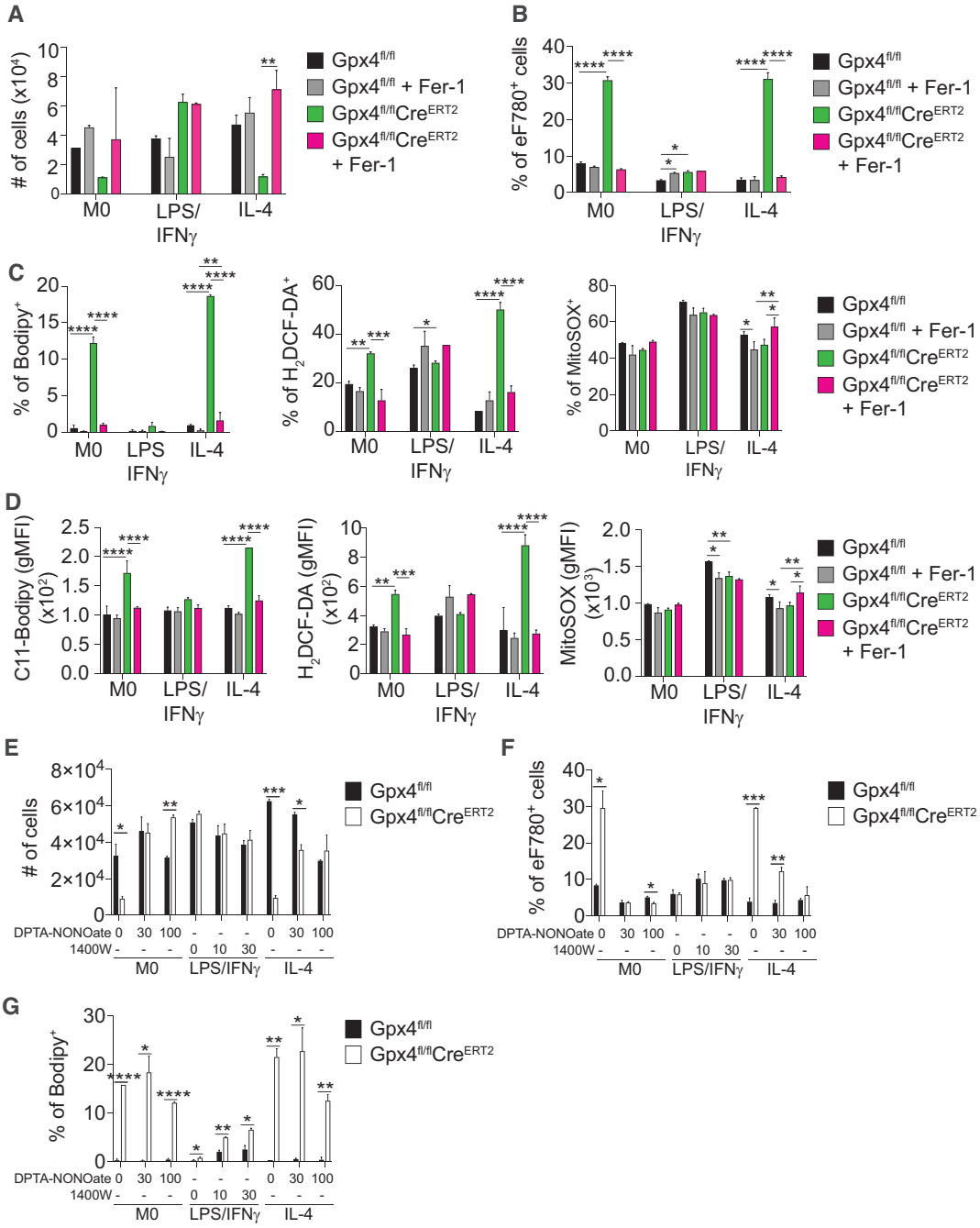

Figure 2. IL-4 stimulation triggers ferroptosis in Gpx4-deficient macrophages. BMDMs were unstimulated (M0) or stimulated with LPS (20 ng/mL) plus IFN-γ (50 ng/mL) or IL-4 (20 ng/mL) in the presence of ferroptosis inhibitor (Fer-1; 10 μM) (A-D), iNOS inhibitor (1400 W; 10 or 30 μM), or NO donor DPTA-NONOate (30 or 100 μM) (E-G). (A) Total number of viable cells after 24 h. (B) Percentage of dead cells stained with eFluor780 after 24 h. (C-D) Percentage (C) or geometric mean fluorescence intensity (gMFI) (D) of C11-Bodipy$^{581/591}$, H_2DCF-DA, or MitoSOX. (E) Quantification of viable cells after 24 h. (F) Percentage of dead cells stained with eFluor780 after 24 h. (G) Percentage of C11-Bodipy$^{581/591+}$ after 6 h. All data were obtained by flow cytometry. Error bars indicate mean ±SD. $^{*}p < 0.05$; $^{**}p < 0.01$; $^{***}p < 0.001$; $^{****}p < 0.0001$ (two-tailed Student's *t*-test). Data are representative of two independent experiments with two to three samples per experiment.

analyzed ROS accumulation after 6 h of stimulation, a time point at which viability was unaffected (data not shown). In unstimulated and IL-4-stimulated Gpx4$^{fl/fl}$Cre^{ERT2} cells, both lipid and cellular ROS levels were elevated as measured by C11-BODIPY$^{581/591}$ and H_2DCF-DA, respectively, and were suppressed to levels equivalent to controls in the presence of Fer-1 (Fig. 2C and D, Supporting information Fig. S2A). Mitochondrial ROS detected by MitoSOX was unaltered by the absence of Gpx4 or in the presence of Fer-1 (Fig. 2C and D, Supporting information Fig. S2A). Consistent with the lack of effects on viability in LPS/IFN-γ-stimulated

$Gpx4^{fl/fl}Cre^{ERT2}$ cells, ferroptosis was not detected under this condition. To check for the accumulation of dysfunctional mitochondria showing a loss of mitochondrial membrane potential, we costained with Mitotracker Green for total mitochondrial mass and Mitotracker Deep Red for mitochondrial membrane potential. We observed no difference in dysfunctional mitochondria (Mitotracker $Green^{+}$, Mitotracker Deep $Red^{-/low}$) (Supporting information Fig. S2B). Together, these data suggest that Gpx4-deficiency results in ferroptosis in M0 and AAM but not in inflammatory macrophages.

To further prove that death in AAM occurs by ferroptosis, we tested the efficiency of various ROS scavengers to prevent death upon polarization with IL-4. In addition to Fer-1, only iron chelator deferoxamine and Vitamin E (α-tocopherol) could efficiently reduce IL-4-induced mortality, while other ROS scavengers, such as *N*-acetylcysteine, Vitamin C (ascorbic acid, AA), or diphenyleneiodonium were unable to prevent cell death (Supporting information Fig. S2C). These results confirm that in vitro death of polarized macrophages occurs by ferroptosis. Additionally, we measured mRNA of other genes that are associated with ferroptosis such as prostaglandin-endoperoxide synthase 2 (*Ptgs2*) and *Slc7a11*. *Ptgs2*, also known as COX-2, has been shown to be upregulated in cancer cells upon treatment with ferroptosis inducers [16]. In addition, *Ptgs2* is known to be induced upon macrophage stimulation with LPS/IFN-γ [23]. We found that *Ptgs2* expression was potently and selectively upregulated in LPS/IFN-γ−stimulated BMDM, consistent with a previous report [23], irrespective of Gpx4 expression (Supporting information Fig. S2D). Inhibition of *Slc7a11* is a well-known driver of ferroptosis in cancer cells [21]. Similar to *Ptgs2*, *Slc7a11* expression was induced upon LPS/IFN-γ but not on IL-4 stimulation in control BMDMs. Notably, absence of Gpx4 induced a significant increase in *Slc7a11* levels in M0 and AAM. TLR engagement and proinflammatory cytokines induce the expression of iNOS in macrophages, which is important for the production of NO and consequently, reactive nitrogen species [24]. LPS/IFN-γ stimulation of Gpx4-deficient macrophages upregulates iNOS expression (Fig. 1E, Supporting information Fig. S1D) without the induction of ferroptosis. To explore this protective mechanism against ferroptosis in Gpx4-deficient inflammatory macrophages, we inhibited iNOS using 1400 W in inflammatory macrophages, and conversely added NO donating compound dipropylenetriamine NONOate (DPTA-NONOate) to M0 and AAM. Varying concentrations of 1400 W in inflammatory macrophages had no effect on viability of LPS/IFN-γ-stimulated BMDM. However, DPTA-NONOate restored survival in Gpx4-deficient M0 and AAM to levels equivalent to that of controls (Fig. 2E and F). This sustained viability in $Gpx4^{fl/fl/}Cre^{ERT2}$ AAM also correlated with decreased lipid peroxidation, a hallmark of ferroptosis (Fig. 2G and Supporting information Fig. S2E). As expected, iNOS inhibition had a minimal effect on lipid peroxidation levels in Gpx4-deficient inflammatory macrophages. These results suggest that while NO confers protection from ferroptosis in AAM, iNOS is not essential to prevent ferroptosis in Gpx4-deficient inflammatory macrophages.

Gpx4 is dispensable for maintenance of tissue-resident macrophages at steady-state in vivo

Mice lacking Gpx4 in all T-cell and B-cell lineages showed a loss of double-negative thymocytes, peripheral activated T cells, as well as innate-like B1 and marginal zone B cells due to ferroptosis [17, 18]. To address the role of Gpx4 in development and function of myeloid cells in vivo, we crossed $Gpx4^{fl/fl}$ mice with both CD11c-cre and LysM-cre mice. The resulting $Gpx4^{fl/fl}LysM^{cre}CD11c^{cre}$ mice lack Gpx4 across several myeloid subsets, including conventional DCs, monocyte-derived DCs, macrophages, and neutrophils. Strikingly reduced expression of Gpx4 mRNA was found in lung myeloid populations, indicating an efficient deletion (Fig. 3A). FACS analyses of lung, peritoneal lavage (PEL), spleen, and BM showed no difference in $CD45^{+}$ cellularity (Fig. 3B). Accordingly, total number of alveolar macrophages (AM), large peritoneal macrophages (LPM), splenic and BM macrophages were comparable in $Gpx4^{fl/fl}LysM^{cre}CD11c^{cre}$ mice compared to littermate controls (Fig. 3C–E, gating strategies in Supporting information Fig. S3A-C). Number of splenic DCs also remained unaffected in the absence of Gpx4. Although neutrophils in the BM were slightly increased in numbers (Fig. 3F; gating strategy in Supporting information Fig. S3D), frequencies remained intact (Fig. 3G and H; gating strategy in Supporting information Fig. S3E).

We validated the specificity of the LysM-Cre activity for targeting macrophages, monocytes, and neutrophils by assessing the expression of red fluorescence protein (RFP) in various tissues of LysM-Cre mice crossed to Rosa26-RFP mice (Supporting information Fig. S4A and B). The proportion of RFP^{+} in tissue-resident macrophages, such as LPM in the peritoneal cavity, AM in the lung, and fat macrophages, was over 70%, while both monocytes and neutrophils revealed poor expression in the peritoneal cavity, lung, and liver. Furthermore, Gpx4 deletion in peritoneal macrophages from naïve, *Listeria monocytogenes*-infected, or IL-4 hydrodynamic injected $Gpx4^{fl/fl}LysM^{cre}$ mice was verified both at RNA (Supporting information Fig. S4C) and at protein levels in peritoneal macrophages and AMs (Supporting information Fig. S4D-F). Protein depletion was confirmed also in $Gpx4^{fl/fl}Cre^{ERT2}$ mice after tamoxifen injection (Supporting information Fig. S4F-H). Thus, in contrast to M0 BMDM, these results suggest that Gpx4 is dispensable for differentiation, homeostasis, and survival of steady-state resident macrophages in lung, peritoneum, and spleen.

Gpx4 supports in vivo expansion and survival of AAM

We next explored the consequences of in vivo macrophage activation following conditional deletion of Gpx4 in myeloid cells. Hydrodynamics-mediated gene delivery provides an efficient model to overexpress cytokines in vivo [25]. We used this technique to overexpress IL-4 in $Gpx4^{fl/fl}LysM^{cre}$ mice. Four days postinjection, we analyzed cells from the peritoneal cavity (gating strategy Supporting information Fig. S5A). To prove the

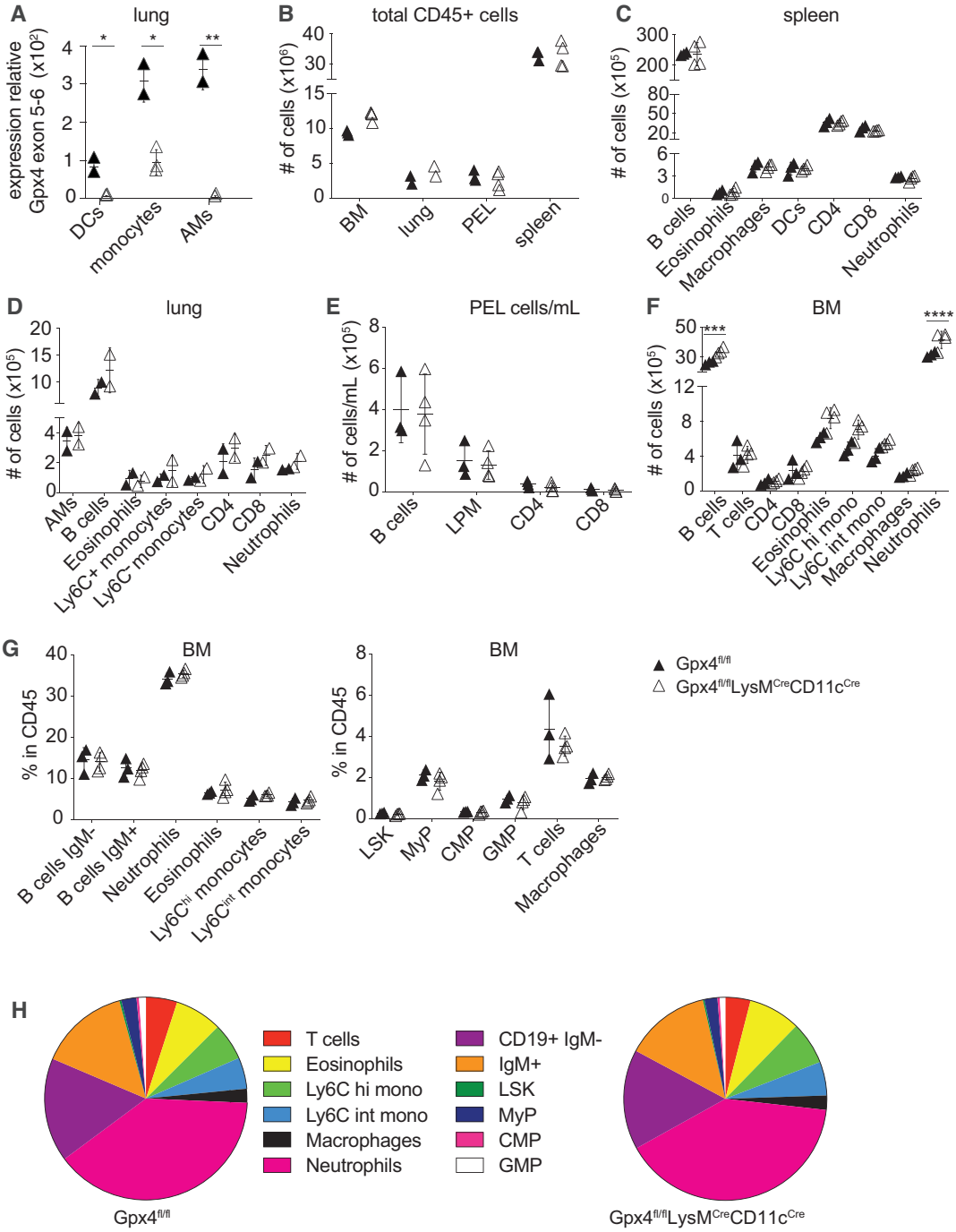

Figure 3. Intact homeostasis of mature myeloid populations in the absence of Gpx4. Naïve Gpx4$^{fl/fl}$CD11c^{cre}LysM^{cre} and Gpx4$^{fl/fl}$ mice at 15 weeks of age. (A) Relative expression of Gpx4 in FACS sorted dendritic cells (DCs), monocytes, and alveolar macrophages (AMs) from the lung by RT-PCR. Data were normalized to TATA-Box Binding Protein. (B) Total number of CD45^{+} cells from the bone marrow (BM), lung, peritoneal lavage (PEL), and spleen by flow cytometry. (C-F) Total cell number of indicated populations in the spleen (C), lung (D), peritoneal cavity (E), and BM (F) by flow cytometry. (G-H) Flow cytometry quantification of immune cell subsets in BM. Error bars indicate mean ±SD. *$p < 0.05$, **$p < 0.01$, ***$p < 0.001$, and ****$p < 0.0001$ (two-tailed Student's *t*-test in [A] and two-way ANOVA in [B-G]). Data are representative of two independent experiments with two (lungs) or four (BM, PEL, and spleen) biological samples per experiment.

efficiency of IL-4 plasmid, we first measured macrophage expansion and polarization in WT mice (Supporting information Fig. S5B). Compared to empty vector controls, mice injected with IL-4 reported a massive expansion of LPM and upregulation of AAM markers, RELMα, and CD301. IL-4-driven expansion of LPM was reduced in Gpx4$^{fl/fl}$LysM^{cre} mice (Supporting information Fig. 4A and B). Expression of AAM marker RELMα was comparable to littermate controls (Supporting information Fig. 4C and D).

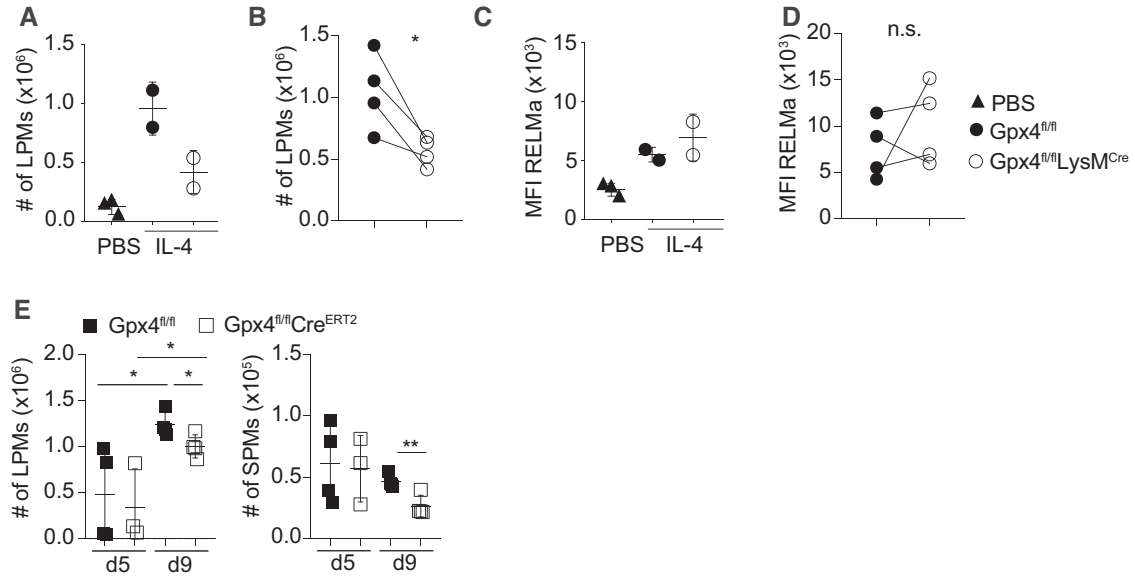

Figure 4. In vivo survival of Gpx4-deficient AAMs is impaired. (A-D) AAM differentiation was induced in Gpx4$^{fl/fl}$ and Gpx4$^{fl/fl}$LysM^{Cre} mice by i.v. hydrodynamic injection of IL-4 plasmid and analyzed 4 days later. (A-B) Flow cytometry quantification of large peritoneal macrophages (LPM). (B) Compiled data from independent experiments with each dot representing mean of one experiment. (C-D) MFI of Relmα in LPM by flow cytometry. (D) Compiled data from independent experiments, each dot represents mean of one experiment. (E) Gpx4$^{fl/fl}$ and Gpx4$^{fl/fl}$Cre^{ERT2} mice were inoculated subcutaneously with 500 *N. brasiliensis* L3 and analyzed 5 and 9 days later. Absolute number of LPM and small peritoneal macrophages (SPMs) by flow cytometry. Error bars indicate mean ±SD. $^{*}P < 0.05$; $^{**}P < 0.01$ (two-tailed Student's *t*-test in [E] and paired *t*-test in [B and D]). Data are representative of four (A-D) and three (E) independent experiments with two to four (A-D), three to four (E) biological samples per experiment.

Similarly, CD301 (Supporting information Fig. S5C) and PD-L2 (Supporting information Fig. S5D) were unchanged. These results suggest that Gpx4 supports proliferation and/or survival but is not essential for differentiation to AAM.

Next, we sought to evaluate the function of Gpx4 in type 2-dependent immunity. We deleted Gpx4 in mice using intraperitoneal tamoxifen injection, infected the mice with *Nippostrongylus brasiliensis* larvae, and analyzed macrophages in the peritoneal cavity after 5 and 9 days. While small peritoneal macrophages (SPM) and LPM were present in comparable numbers at day 5, when the larvae arrive in the intestines, both populations were reduced in numbers in Gpx4$^{fl/fl}$Cre^{ERT2} mice (Fig. 4E) at day 9, highlighting a role of Gpx4 for survival of macrophages during type 2 immunity.

To investigate the function of inflammatory macrophages in vivo, we used Th1-type infection models to study the host resistance to pathogens in Gpx4 KO mice. First, we challenged Gpx4$^{fl/fl}$LysM^{cre} with Gram-positive *L. monocytogenes*. Gpx4$^{fl/fl}$LysM^{cre} revealed comparable bacterial load to littermate control mice in the spleen and liver 2 days postinfection (Fig. 5A). Myeloid subpopulations of macrophage, monocyte, and neutrophils numbers were equivalent to controls in the peritoneal cavity of naïve and infected mice (Fig. 5B; gating strategy Supporting information Fig. S5E). We next infected mice with *Leishmania major* parasites in footpads and monitored the swelling weekly as a proxy for the progression of infection. Gpx4$^{fl/fl}$LysM^{cre} and control mice showed similar footpad swelling curves (Fig. 5C), peaking around 3-4 weeks postinfection. Parasite burden in draining lymph node (dLN), spleen, and footpad was comparable to controls at 8 weeks postinfection (Fig. 5D). Total number of immune cells and their proportional subsets in dLN displayed no significant abnormalities (Fig. 5E). In addition, we infused zymosan into the peritoneum to induce peritonitis and analyzed the peritoneal macrophages. We found an overall increase in CD45^{+} cells, as well as an increase in SPM, but not in LPM, in Gpx4$^{fl/fl}$Cre^{ERT2} (Fig. 5F, Supporting information Fig. S5F). Moreover, there was a significantly higher percentage of CD86 and CD206 in LPM of Gpx4$^{fl/fl}$Cre^{ERT2} mice, while SPM displayed no difference (Fig. 5G). Taken together, consistent with BMDM results in vitro, these data indicate that Gpx4 is dispensable for generation of proinflammatory macrophages and myeloid cells allowing protection from intracellular infections, but has a significant role on sustaining the survival of AAM in type 2 responses.

Discussion

Redox regulation is essential to tightly control the balance between ROS production and antioxidant protection. Although excessive ROS induce adverse mutagenesis and cell death, they can act as secondary messengers at low levels to alter cell function by protein oxidation [6, 7]. Moderate concentrations of mitochondrial ROS are crucial for microbial defense [26], and determine the inflammatory phenotype of macrophages [27]. Macrophage activation by TLR engagement stimulates a ROS-induced signal transduction cascade that triggers inflammatory mediators such as NF-κB activation, HIF-1α stabiliza-

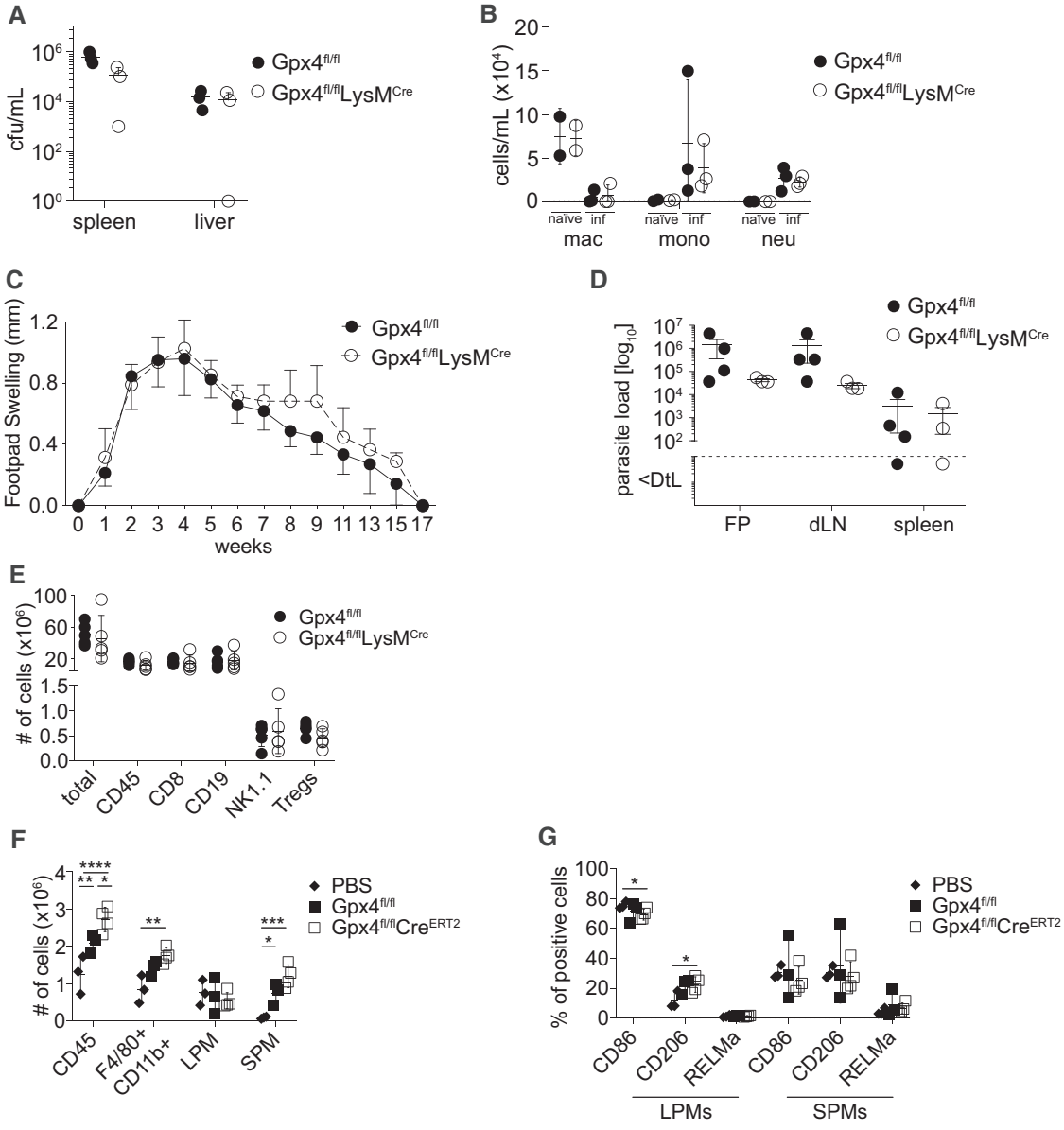

Figure 5. In vivo survival of Gpx4-deficient inflammatory macrophages is unaffected. (A, B) Gpx4$^{fl/fl}$ and Gpx4$^{fl/fl}$LysM^{cre} mice were infected i.p. with 5×10^4 colony forming units (cfu) of *L. monocytogenes* and analyzed at 2 days postinfection. (A) CFU was determined in spleen and liver. (B) Absolute number of macrophages (mac), monocytes (mono), and neutrophils (neu) from the peritoneal cavity of naïve and infected mice by flow cytometry. (C-E) Gpx4$^{fl/fl}$ and Gpx4$^{fl/fl}$LysM^{cre} mice were infected with 2×10^6 *L. major* parasites subcutaneously. (C) Measured swelling of infected footpad compared to uninfected baseline at indicated weeks postinfection. (D) Parasite load in footpad (FP), popliteal draining lymph node (dLN), and spleen at 8 weeks postinfection as determined by limiting dilution analysis. (E) Flow cytometry quantification of immune subsets in popliteal dLN. (F-G) Gpx4$^{fl/fl}$ and Gpx4$^{fl/fl}$Cre^{ERT2} mice were injected with zymosan A (100 mg/kg mouse) intraperitoneally and analyzed at 3 days postinjection. (F) Flow cytometry of subpopulations from peritoneal cavity. (G) Percentage of CD86$^+$, CD206$^+$ and Relmα^+ in peritoneal macrophages by flow cytometry. Error bars indicate mean ±SD. $^*p < 0.05$; $^{**}p < 0.01$; $^{***}p < 0.001$; $^{****}p < 0.0001$ (two-tailed Student's *t*-test [A, D], two-way ANOVA [B, E, F and G]). Data are representative of four (A-B), three (C-E), and two (F-G) independent experiments with two to three (A, B), 10 (C), three to four (D-G) biological samples per experiment.

tion, and inflammatory cytokine production [28–30]. Therefore, ROS are not only crucial effector molecules for inflammatory macrophages, but also play a vital role in activation and differentiation. Here, we analyze the defense mechanism against lipid peroxidation in myeloid cells and demonstrate that the antioxidant enzyme Gpx4 has a distinct regulatory function within myeloid subpopulations.

This study adds to a growing body of evidence showing that antioxidant defense by Gpx4 is critically required to prevent ferroptosis. We also show that Gpx4 requirement in vivo is not uniform among macrophage subsets but rather restricted to AAM. Although M0 macrophages lacking Gpx4 were also susceptible to ferroptosis in vitro, the development and homeostasis of Gpx4-deficient tissue-resident macrophages in lung, peritoneum,

spleen, and BM, which may be considered as M0 status, was unaffected in vivo. It is noteworthy, however, that the subsequent decrease in number of AAM upon Gpx4 deletion may be prompted by reduced proliferation or expansion. Strikingly, inflammatory macrophages that produce ROS for oxidative burst remained largely unaffected by the absence of Gpx4 in vitro and in several infectious disease models associated with potent proinflammatory macrophage responses. Despite acquiring cellular ROS as a consequence of inflammatory stimuli, we found no difference in activation, function, or survival of inflammatory macrophages in microbial infections, indicating that other antioxidant mechanisms contribute to avert ROS accumulation in these cell types. These findings are consistent with the observation that $Gpx4^{fl/fl}LysM^{cre}$ mice have a comparable tumor burden and sustain survival despite higher ROS levels [31]. Recent study suggested that iNOS expression in inflammatory macrophages negatively regulates the onset of ferroptosis [32]. Although we found that NO supplementation protected AAM lacking Gpx4 from ferroptosis, we were unable to induce ferroptosis in inflammatory macrophages through iNOS inhibition. This result argues against the previously reported interpretation, suggesting other protective mechanisms for inflammatory macrophages. We hypothesize that metabolic reprogramming may play an important role in promoting ferroptosis and thereby dictating the requirement for Gpx4. Cell activation is associated with dynamic metabolic changes and mitochondria play a central role in the regulation of cellular energy. Mitochondrial TCA cycle is used for ATP synthesis in quiescent and AAM. Inflammatory macrophages switch to aerobic glycolysis and mitochondria are repurposed for ROS production [27, 33]. Furthermore, production of NO via upregulation of iNOS expression inhibits mitochondrial respiration by nitrosylating iron-sulfur proteins within complex I of the electron transport chain [34], thereby inhibiting mitochondrial metabolism and supporting glycolysis. Glutamine metabolism is another important fuel source that supports the TCA cycle, particularly in AAM [35]. Glutaminolysis and electron transport chain have been implicated as a source of ferroptosis, although ferroptosis has been linked to absence of glutamine in Gpx4-deficient cell lines [36]. We tested the viability of LPS and LPS-/IFN-γ-treated Gpx4-deficient macrophages with glutaminolysis inhibitor BPTES but found no link to ferroptosis induction (data not shown). Further work is necessary to assess the contribution of mitochondrial respiration and ferroptosis.

Activation of the inflammasome pathway is one of the protective mechanisms in innate immunity and is characterized by proteolytic maturation of proinflammatory cytokine IL-1β and induction of pyroptosis [37, 38]. Gpx4 has been implicated as a negative regulator of pyroptosis as Gpx4 deletion in myeloid cells increased production of IL-1β and susceptibility to gasdermin-D-mediated septic lethality [19]. Contrary to this finding, we did not observe any differences in IL-1β secretion through canonical NLRP3, as well as AIM2 and NLRC4 inflammasome pathways. Although caspase-11 initiates the noncanonical inflammasome pathway, maturation of IL-1β is dependent on caspase-1 in both canonical and noncanonical pathways [39]. Therefore, this discrepancy in IL-1β secretion by Gpx4-deficient macrophages will need to be addressed in future studies.

Collectively, our findings suggest that IL-4-driven macrophage activation critically affects the cellular redox balance and Gpx4 assumes an integral role in lipid ROS scavenging. Loss of Gpx4 activity in IL-4-driven macrophage differentiation leads to ferroptotic cell death, but not in inflammatory macrophages, which were able to sustain cell survival and function. This demonstrates that antioxidant defense regulation in macrophages is not uniform but rather is controlled differentially among myeloid subsets in homeostasis and activation. Rational targeting of this gene, therefore, holds therapeutic potentials to combat genetic disorders and pathologies driven by lipid peroxidation.

Materials and methods

Mice

$Gpx4^{fl/fl}LysM^{cre}$, $Gpx4^{fl/fl}CD11c^{cre}$, and $Gpx4^{fl/fl}Cre^{ERT2}$ mice were generated by crossing $Gpx4^{fl/fl}$ mice [14] to LysM-Cre (JAX 004781) [40], CD11c-Cre (JAX stock 008068) [41], or Ert2-Cre [42] mice, respectively. C57BL/6 mice were originally from the Jackson Laboratory (Bar Harbor, Maine, USA). LysM-cre mice were crossed to Rosa26-RFP mice [43]. All mice were crossed for at least 10 generations to C57BL/6. Experiments were performed with age and sex matched animals. Experimental mice ages ranged from 6-15 weeks. All animal experiments were performed according to the institutional guidelines and Swiss federal regulations and were approved by the animal ethics committee of Kantonales Veterinärsamt, Zürich, Switzerland (permission no. ZH161/15, ZH134/18, ZH054/18).

In vivo tamoxifen administration

For each mouse, 2 mg of tamoxifen (Sigma) was dissolved in 40 μL of ethanol (Sigma) and subsequently mixed with 40 μL cremofor (Sigma). A total of 320 μL of PBS was added on top and 400 μL was injected i.p. in mice. At least two injections were performed on nonconsecutive days. Injections were performed 5 and 2 days before the analysis or before starting the treatment. For *N. brasiliensis*, mice were injected with one shot of tamoxifen the day before infection and later given tamoxifen by oral gavage every other day (from +d1). For this regime, tamoxifen was dissolved in corn oil (Sigma) to a concentration of 20 mg/mL. Injected volume was adjusted to give 0.2 mg/g of body weight.

Isolation of single cells from organs

Mice were sacrificed by CO_2 asphyxiation or injection of overdose (400 mg/kg of body weight) sodium pentobarbital (i.p. or i.v.). PEL was collected with 5 mM EDTA in DPBS (Thermo Fisher). AMs were isolated by washing the lungs three times with 0.4

mL of ice-cold PBS containing 2 mM EDTA through an intratracheal cannula. All organs except the lung were removed prior to heart perfusion with DPBS. Lungs were digested for 45 min at 37°C in IMDM (Thermo Fisher) with 2 mg/mL of type IV collagenase (Worthington) and 0.02 mg/mL of type I DNase (Sigma). BM cells were flushed from tibias and femurs and passed through a 70-μm strainer (Corning). All other organs were directly passed through 70-μm strainer. Red blood cell lysis was performed with ACK buffer (0.15 M NH_4Cl, 1 mM $KHCO_3$, and 0.1 mM EDTA) on spleen and BM cells.

Preparation and activation of BMDM

BM cells were isolated from the femur and tibia of mice and dissociated into single-cell suspension by filtration through 70-μm strainer. Red blood cells were lysed with ACK lysis buffer and BM cells were cultured in vitro in the presence of recombinant mouse M-CSF (20 ng/mL; Peprotech) in complete RPMI-1640 medium (containing 10 mM glucose, 2 mM L-glutamine, 100 U/mL of penicillin-streptomycin and 10% heat-inactivated FBS [Sigma Aldrich]) for 7 days. M-CSF was replenished on day 3 and 5. In vitro Gpx4 deletion in $Gpx4^{fl/fl}Cre^{ERT2}$ mice was performed by supplying 5 μM tamoxifen on day 3 and 5. At day 7, viable cells were counted with trypan blue staining, and were plated at 100 000 cells/well. Activation was carried out in the absence of M-CSF. Cells were stimulated with LPS (20 or 100 ng/mL), CpG (80 or 100 nM), R837 (5 μg/mL), Zymosan (20 μg/mL), IL-4 (20 ng/mL; PeproTech), or IFN-γ (50 ng/mL; PeproTech) in the presence of iNOS inhibitor (1400 W; 10 or 30 μM) ferroptosis inhibitor Fer-1 (10 μM; ChemBridge), deferoxamine (100 μM), Vitamin E (α-tocopherol; 10 μM), *N*-acetylcysteine (NAC; 800 μM), Vitamin C (AA; 4 μM), diphenyleneiodonium (2 μM), or NO donor DPTA-NONOate (30 or 100 μM) for 6, 24, or 48 h. To assess proliferation, cells were incubated with 5-ethynyl-2'–deoxyuridine (EdU; 75 μM; Thermo Fisher) for 24 h. Reagents were purchased from Sigma-Aldrich unless otherwise stated.

For inflammasome activation, BMDMs were stimulated with LPS for 16-18 h. Cells were additionally stimulated with adenosine triphosphate (2 mM) for 2 h to activate NLRP3 inflammasome. Poly(dA:dT) (1 μg/mL; Sigma) was transfected using Lipofectamine 2000 (Invitrogen) in accordance with the manufacture's protocol to activate AIM2-mediated inflammasome. LFn-FlaA, LFn-FlaA(AAA) were kind gifts from Dr. Russell E. Vance (UC Berkeley), and were purified as previously described [44]. DetoxiGel (Pierce) was used to remove endotoxin according to manufacturer's protocol. To activate NLRC4 inflammasome, BMDMs were stimulated additionally with anthrax protective antigen (PA, 10 μg/mL; Merck) and purified LFn-FlaA (5 μg/mL) or LFn-FlaA(AAA) (5 μg/mL) for 1 h. Cell supernatants were harvested for IL-1β detection.

Nitric oxide production assay

Day 7 BMDMs were stimulated in the presence of IFN-γ (20 ng/mL; PeproTech) with either LPS (100 ng/mL), R837 (2.5 μg/mL), CpG (1 μM), or Poly I:C (40 μg/mL) for 6 h. Supernatants were removed and subjected to Griess Assay (homemade). All reagents were purchased from Sigma–Aldrich unless stated otherwise.

Cytokine detection with ELISA

Cytokine concentrations in cell culture supernatants were determined by sandwich ELISA using the following antibodies (eBioscience): IL-1β (14-7012-85 and 13-7112-85), IL-6 (14-8061-62 and 13-7062-85), IL-12 (14-7125-85 and 13-7123-85), and TNF-α (14-8321 and 13-7341-85).

Flow cytometry

Viable cells were stained with eFluor780 (eBioscience), Zombie Aqua (Biolegend), or Sytox green (Thermo Fisher) diluted in PBS for 30 min at 4°C and blocked with anti-CD16/32 (homemade) prior to cell surface staining. Cells were stained in PBS containing 2% heat-inactivated FBS and 2 mM EDTA at 4°C. Antibodies used were as follows: anti-CD206 (C068C2; L138D7) anti-CD301 (LOM-8.7; URA-1), anti-PDL2 (TY25), anti-F4/80 (BM8), anti-CD11c (N418), anti-CD11b (M1/70), anti-Siglec F (E50-2440; BD Bioscience), anti-I-A/I-E (M5/114.15.2), anti-CD45 (30-F11), anti-CD4 (RM4-5; GK1-5 eBioscience), anti-CD8 (53-6.7; eBioscience), anti-CD45.1 (A20), anti-CD45.2 (104), anti-Ly6G (1A8), anti-Ly6C (HK1.4), anti-GR1 (RB6-8C5), anti-Ter119 (TER-119; eBioscience), anti-TCRβ (H57-507), anti-CD19 (6D5), anti-CD34 (SA376A4), anti-B220 (RA3-6B2), anti-Sca1 (D7; BD Bioscience), anti-cKit (2B8), anti-CD16/32 (93; eBioscience), streptavidin (563262; BD Bioscience). For intracellular staining, cells were fixed in 4% paraformaldehyde and were stained for 1 h at 25°C with anti-RELMα (500-P214; PeproTech), anti-Gpx4 (EPNCIR144; Abcam) and anti-NOS2 (M19; Santa Cruz Biotechnology) in 0.5% saponin buffer. Cells were further stained with anti-rabbit IgG (Southern Biotech). All antibodies were purchased from Biolegend unless noted otherwise. For ROS and mitochondrial dyes, cells were labeled with 5 μM MitoSOX, 1 μM H_2DCF-DA, 2 μM C11-$Bodipy^{581/591}$, and 20 nM mitotracker green and deep red according to manufacturers' protocol. Lipid peroxidation was determined by oxidation of C11 measured on 488 nm laser (green emission at 530/30). Click-iT EdU was detected according to manufacturers' protocol. All dyes were purchased from Thermo Fisher. Data were acquired at a minimum of 100,000 cells on FACSCanto II or LSRFortessa (BD Biosciences), FACS sorted with FACSAria III (BD Bioscience), and were analyzed with FlowJo software version 10 (TreeStar).

Real-time RT-PCR analysis

Total RNA was extracted using TRI Reagent (Invitrogen), followed by reverse transcription using GoScript RT (Promega). Quantitative real-time RT-PCR was performed using Brilliant SYBR Green

(Stratagene) on an i-Cycler (Bio-Rad Laboratories) according to manufacturers' protocol. Relative expression was normalized to the housekeeping genes TBP-F (5' – TTG ACC TAA AGA CCA TTG CAC TTC – 3') and TBP-R (5' – TTC TCA TGA TGA CTG CAG CAA A – 3') or EF-1α-F (5'-TCCACTTGGTCGCTTTGCT-3') and EF-1α-R (5'-CTTCTTGTCCACAGCTTTGATGA-3'). Primer sequences are as follows: Arg1-F (5' – ACC TGG CCT TTG TTG ATG TCC CTA – 3'), Arg1-R (5' – AGA GAT GCT TCC AAC TGC CAG ACT – 3'), Fizz1-F (5' – TCC AGC TGA TGG TCC CAG TGA ATA – 3'), Fizz1-R (5' – ACA AGC ACA CCC AGT AGC AGT CAT – 5'), Ym1-F (5' – AGA AGG GAG TTT CAA ACC T – 3'), Ym1-R (5' – GTC TTG CTC ATG TGT GTA AGT GA – 3'), Gpx4-F (5' – CTG TGG AAA TGG ATG AAA G – 3'), Gpx4-R (5' – TCA ATG AGA AAC TTG GTA AAG – 3'), Ptgs2-F (5' – TGT GAA CAA CAT CCC CTT CC – 3'), Ptgs2-R (5' – GTC ATG CGC TGA GTT GTA GG – 3'), Slc7a11-F (5' – GCT CGT AAT ACG CCC TGG AGC – 3'), and Slc7a11-R (5' – CGA GCT TGA TTG CAA GTT CAG G – 3').

Hydrodynamic overexpression of IL-4

For hydrodynamic gene delivery, the mouse IL-4 coding sequence was cloned into pTT5 expression vector. Plasmid DNA was purified using the Maxi-prep kit (Zymo Research) and adjusted to 10 mg/mouse in sterile DPBS (Thermo Fisher) in total volume (mL) of 10% of body weight (g). Mice were injected intravenously and monitored daily until euthanized.

L.monocytogenes, *L. major*, and *N. brasiliensis* infections

Listeria monocytogenes (LM10403S) was cultured in brain heart infusion (BHI; Sigma Aldrich) at 37°C and was grown to log-phage measured by OD at 600 nm. $Gpx4^{fl/fl}$ and $Gpx4^{fl/fl}LysM^{cre}$ mice at 7 weeks of age were infected intraperitoneally with 50 000 cfu and sacrificed 2 days postinfection. Temperature and weight of individual mice were measured over the course of the infection. Bacterial load was determined from spleen, liver, and PEL cells by tenfold serial dilutions on BHI agar incubated at 37°C overnight.

For cutaneous leishmaniasis, *Leishmania major* parasites (MHOM/IL/81/FEBNI) were grown in complete Schneider's Drosophila Medium (Invitrogen) with 20% heat-inactivated FBS, 100 U/mL penicillin 6-potassium, and 100 μg/mL streptomycin sulfate for 7 days at 27°C. Metacyclic promastigote parasites were purified using peanut lectin agglutination (Sigma–Aldrich) as previously described [45]. $Gpx4^{fl/fl}$ and $Gpx4^{fl/fl}LysM^{cre}$ mice at 7 weeks of age were infected with 2×10^6 parasites into the right hind footpad and footpad swelling was measured weekly for 17 weeks, while a portion of the group was euthanized for analysis 8 weeks postinfection. To quantify parasite load in the footpad, spleen and draining popliteal lymph node (dLN), single-cell suspensions were plated on 96-well plates across a threefold serial dilution in complete Schneider's Drosophila Medium at 27°C. Parasite growth was determined after 7 days of incubation. For analysis of immune cell populations, single-cell suspensions from dLN were used for FACS analysis.

For *Nippostrongylus brasilliensis* infection, infective third-stage larvae (L3) were washed extensively in sterile PBS and 500 live L3 were injected subcutaneously into loose skin at the base of the tail of $Gpx4^{fl/fl}$ and $Gpx4^{fl/fl}Cre^{ERT2}$ mice. Five and nine days postinfection, PEL was harvested for FACS analysis.

Zymosan-induced peritonitis

Peritoneal inflammation was induced by intraperitoneal injection of zymosan A (from *Saccharomyces cerevisiae*, Sigma) at 100 mg/kg to $Gpx4^{fl/fl}$ and $Gpx4^{fl/fl}Cre^{ERT2}$ mice at 8 weeks of age. PEL was collected 3 days postzymosan injection and analyzed for macrophage populations by FACS.

Statistical analysis

GraphPad Prism 8 software was used for representations and statistical analysis. Student's *t*-test was used for comparison of two groups, paired *t*-test was used to compare pooled experiments. One- or two-way ANOVA and Tukey's correction was used for comparison of more than two groups within the same experiment.

Acknowledgments: We thank the ETH Flow Cytometry Core facility technical support for cell sorting. We are grateful to Georg Bornkamm and Marcus Conrad for providing us with $Gpx4^{fl/fl}$ mice. This work was supported by grants from Novartis Foundation for Medical-Biological Research (15B140) and Swiss National Science Foundation (310030B_182829) to MK, Peter Hans Hofschneider Professorship for Molecular Medicine and Foundation for Research in Science and the Humanities at the University of Zurich (STWF-20-007) to CS.

Conflict of interest: The authors have no declare no financial conflict of interest.

Ethics approval statement for animal studies: All animal experiments were performed according to the institutional guidelines and Swiss federal regulations and were approved by the animal ethics committee of Kantonales Veterinärsamt, Zürich, Switzerland (permission no. ZH161/15, ZH134/18, ZH054/18).

Guidelines for flow cytometry analysis: The authors adhered to the guidelines for analysis of flow cytometry analysis [46].

Authors' contributions: MM and FP designed and performed majority of experiments and analyzed data. PB, JM, and XF performed specific experiments. CS gave valuable advice. FP, MM, and MK wrote the manuscript. MK conceived the ideas, oversaw the research program, and received funding.

Data availability statement: The data that support the findings of this study are available from the corresponding author upon reasonable request.

Peer review: The peer review history for this article is available at https://publons.com/publon/10.1002/eji.202049114

References

1 **Janeway, C. A., Jr.** and **Medzhitov, R.**, Innate immune recognition. *Annu. Rev. Immunol.* 2002. **20**: 197–216.

2 **Gordon, S.** and **Taylor, P. R.**, Monocyte and macrophage heterogeneity. *Nat. Rev. Immunol.* 2005. **5**: 953–964.

3 **Wynn, T. A.**, **Chawla, A.** and **Pollard, J. W.**, Macrophage biology in development, homeostasis and disease. *Nature* 2013. **496**: 445–455.

4 **Kumar, H.**, **Kawai, T.** and **Akira, S.**, Toll-like receptors and innate immunity. *Biochem. Biophys. Res. Commun.* 2009. **388**: 621–625.

5 **Leto, T. L.** and **Geiszt, M.**, Role of Nox family NADPH oxidases in host defense. *Antioxid. Redox. Signal.* 2006. **8**: 1549–1561.

6 **Sena, L. A.** and **Chandel, N. S.**, Physiological roles of mitochondrial reactive oxygen species. *Mol. Cell.* 2012. **48**: 158–167.

7 **D'Autréaux, B.** and **Toledano, M. B.**, ROS as signalling molecules: mechanisms that generate specificity in ROS homeostasis. *Nat. Rev. Mol. Cell. Biol.* 2007. **8**: 813–824.

8 **Lin, M. T.** and **Beal, M. F.**, Mitochondrial dysfunction and oxidative stress in neurodegenerative diseases. *Nature* 2006. **443**: 787–795.

9 **Giacco, F.** and **Brownlee, M.**, Oxidative stress and diabetic complications. *Circ. Res.* 2010. **107**: 1058–1070.

10 **Valko, M.**, **Rhodes, C. J.**, **Moncol, J.**, **Izakovic, M.** and **Mazur, M.**, Free radicals, metals and antioxidants in oxidative stress-induced cancer. *Chem. Biol. Interact.* 2006. **160**: 1–40.

11 **Maccarrone, M.** and **Brüne, B.**, Redox regulation in acute and chronic inflammation. *Cell. Death Differ.* 2009. **16**: 1184–1186.

12 **Yant, L. J.**, **Ran, Q.**, **Rao, L.**, **Van Remmen, H.**, **Shibatani, T.**, **Belter, J. G.**, **Motta, L.** et al., The selenoprotein GPX4 is essential for mouse development and protects from radiation and oxidative damage insults. *Free Radic. Biol. Med.* 2003. **34**: 496–502.

13 **Imai, H.**, **Hirao, F.**, **Sakamoto, T.**, **Sekine, K.**, **Mizukura, Y.**, **Saito, M.**, **Kitamoto, T.** et al., Early embryonic lethality caused by targeted disruption of the mouse PHGPx gene. *Biochem. Biophys. Res. Commun.* 2003. **305**: 278–286.

14 **Seiler, A.**, **Schneider, M.**, **Forster, H.**, **Roth, S.**, **Wirth, E. K.**, **Culmsee, C.**, **Plesnila, N.** et al., Glutathione peroxidase 4 senses and translates oxidative stress into 12/15-lipoxygenase dependent- and AIF-mediated cell death. *Cell. Metab.* 2008. **8**: 237–248.

15 **Canli, Ö.**, **Alankuş, Y. B.**, **Grootjans, S.**, **Vegi, N.**, **Hültner, L.**, **Hoppe, P. S.**, **Schroeder, T.** et al., Glutathione peroxidase 4 prevents necroptosis in mouse erythroid precursors. *Blood* 2016. **127**: 139–148.

16 **Yang, W. S.**, **SriRamaratnam, R.**, **Welsch, M. E.**, **Shimada, K.**, **Skouta, R.**, **Viswanathan, V. S.**, **Cheah, J. H.** et al., Regulation of ferroptotic cancer cell death by GPX4. *Cell.* 2014. **156**: 317–331.

17 **Matsushita, M.**, **Freigang, S.**, **Schneider, C.**, **Conrad, M.**, **Bornkamm, G. W.** and **Kopf, M.**, T cell lipid peroxidation induces ferroptosis and prevents immunity to infection. *J. Exp. Med.* 2015. **212**: 555–568.

18 **Muri, J.**, **Thut, H.**, **Bornkamm, G. W.** and **Kopf, M.**, B1 and marginal zone B cells but not follicular B2 cells require Gpx4 to prevent lipid peroxidation and ferroptosis. *Cell. Rep.* 2019. **29**: 2731–2744.

19 **Kang, R.**, **Zeng, L.**, **Zhu, S.**, **Xie, Y.**, **Liu, J.**, **Wen, Q.**, **Cao, L.** et al., Lipid peroxidation drives gasdermin D-mediated pyroptosis in lethal polymicrobial sepsis. *Cell. Host. Microbe.* 2018. **24**: 97–108.

20 **Muri, J.** and **Kopf, M.**, Redox regulation of immunometabolism. *Nat. Rev. Immunol.* 2021. **21**: 363–381.

21 **Dixon, S. J.**, **Lemberg, K. M.**, **Lamprecht, M. R.**, **Skouta, R.**, **Zaitsev, E. M.**, **Gleason, C. E.**, **Patel, D. N.** et al., Ferroptosis: an iron-dependent form of nonapoptotic cell death. *Cell.* 2012. **149**: 1060–1072.

22 **Doll, S.**, **Proneth, B.**, **Tyurina, Y. Y.**, **Panzilius, E.**, **Kobayashi, S.**, **Ingold, I.**, **Irmler, M.** et al., ACSL4 dictates ferroptosis sensitivity by shaping cellular lipid composition. *Nat. Chem. Biol.* 2017. **13**: 91–98.

23 **von Knethen, A.**, **Callsen, D.** and **Brune, B.**, NF-kappaB and AP-1 activation by nitric oxide attenuated apoptotic cell death in RAW 264.7 macrophages. *Mol. Biol. Cell.* 1999. **10**: 361–372.

24 **Bogdan, C.**, Nitric oxide and the immune response. *Nat. Immunol.* 2001. **2**: 907–916.

25 **Jiang, J.**, **Yamato, E.** and **Miyazaki, J.**, Intravenous delivery of naked plasmid DNA for in vivo cytokine expression. *Biochem. Biophys. Res. Commun.* 2001. **289**: 1088–1092.

26 **West, A. P.**, **Brodsky, I. E.**, **Rahner, C.**, **Woo, D. K.**, **Erdjument-Bromage, H.**, **Tempst, P.**, **Walsh, M. C.** et al., TLR signalling augments macrophage bactericidal activity through mitochondrial ROS. *Nature* 2011. **472**: 476–480.

27 **Mills, E. L.**, **Kelly, B.**, **Logan, A.**, **Costa, A. S. H.**, **Varma, M.**, **Bryant, C. E.**, **Tourlomousis, P.** et al., Succinate dehydrogenase supports metabolic repurposing of mitochondria to drive inflammatory macrophages. *Cell.* 2016. **167**: 457–470.

28 **Morgan, M. J.** and **Liu, Z. G.**, Crosstalk of reactive oxygen species and NF-κB signaling. *Cell. Res.* 2011. **21**: 103–115.

29 **Mi, Z.**, **Rapisarda, A.**, **Taylor, L.**, **Brooks, A.**, **Creighton-Gutteridge, M.**, **Melillo, G.** and **Varesio, L.**, Synergystic induction of HIF-1alpha transcriptional activity by hypoxia and lipopolysaccharide in macrophages. *Cell. Cycle.* 2008. **7**: 232–241.

30 **Tannahill, G. M.**, **Curtis, A. M.**, **Adamik, J.**, **Palsson-McDermott, E. M.**, **McGettrick, A. F.**, **Goel, G.**, **Frezza, C.** et al., Succinate is an inflammatory signal that induces IL-1β through HIF-1α. *Nature* 2013. **496**: 238–242.

31 **Canli, Ö.**, **Nicolas, A. M.**, **Gupta, J.**, **Finkelmeier, F.**, **Goncharova, O.**, **Pesic, M.**, **Neumann, T.** et al., Myeloid cell-derived reactive oxygen species induce epithelial mutagenesis. *Cancer Cell.* 2017. **32**: 869–883.

32 **Kapralov, A. A.**, **Yang, Q.**, **Dar, H. H.**, **Tyurina, Y. Y.**, **Anthonymuthu, T. S.**, **Kim, R.**, **St Croix, C. M.** et al., Redox lipid reprogramming commands susceptibility of macrophages and microglia to ferroptotic death. *Nat. Chem. Biol.* 2020. **16**: 278–290.

33 **Pearce, E. L.** and **Pearce, E. J.**, Metabolic pathways in immune cell activation and quiescence. *Immunity* 2013. **38**: 633–643.

34 **Clementi, E.**, **Brown, G. C.**, **Feelisch, M.** and **Moncada, S.**, Persistent inhibition of cell respiration by nitric oxide: crucial role of *S*-nitrosylation of mitochondrial complex I and protective action of glutathione. *Proc. Natl. Acad. Sci. USA* 1998. **95**: 7631–7636.

35 **Liu, P. S.**, **Wang, H.**, **Li, X.**, **Chao, T.**, **Teav, T.**, **Christen, S.**, **Di Conza, G.** et al., α-ketoglutarate orchestrates macrophage activation through metabolic and epigenetic reprogramming. *Nat. Immunol.* 2017. **18**: 985–994.

36 **Gao, M.**, **Yi, J.**, **Zhu, J.**, **Minikes, A. M.**, **Monian, P.**, **Thompson, C. B.** and **Jiang, X.**, Role of mitochondria in ferroptosis. *Mol. Cell.* 2019. **73**: 354–363.

37 **Kayagaki, N.**, **Stowe, I. B.**, **Lee, B. L.**, **O'Rourke, K.**, **Anderson, K.**, **Warming, S.**, **Cuellar, T.** et al., Caspase-11 cleaves gasdermin D for non-canonical inflammasome signalling. *Nature* 2015. **526**: 666–671.

38 **Broz, P.** and **Dixit, V. M.**, Inflammasomes: mechanism of assembly, regulation and signalling. *Nat. Rev. Immunol.* 2016. **16**: 407–420.

39 **Man, S. M.** and **Kanneganti, T. D.**, Gasdermin D: the long-awaited executioner of pyroptosis. *Cell. Res.* 2015. **25**: 1183–1184.

40 **Clausen, B. E.**, **Burkhardt, C.**, **Reith, W.**, **Renkawitz, R.** and **Forster, I.**, Conditional gene targeting in macrophages and granulocytes using LysMcre mice. *Transgenic Res.* 1999. **8**: 265–277.

41 **Caton, M. L.**, **Smith-Raska, M. R.** and **Reizis, B.**, Notch-RBP-J signaling controls the homeostasis of CD8- dendritic cells in the spleen. *J. Exp. Med.* 2007. **204**: 1653–1664.

42 **Hameyer, D.**, **Loonstra, A.**, **Eshkind, L.**, **Schmitt, S.**, **Antunes, C.**, **Groen, A.**, **Bindels, E.** et al., Toxicity of ligand-dependent Cre recombinases and generation of a conditional Cre deleter mouse allowing mosaic recombination in peripheral tissues. *Physiol. Genomics* 2007. **31**: 32–41.

43 **Luche, H.**, **Weber, O.**, **Nageswara Rao, T.**, **Blum, C.** and **Fehling, H. J.**, Faithful activation of an extra-bright red fluorescent protein in "knock-in" Cre-reporter mice ideally suited for lineage tracing studies. *Eur. J. Immunol.* 2007. **37**: 43–53.

44 **Krantz, B. A.**, **Melnyk, R. A.**, **Zhang, S.**, **Juris, S. J.**, **Lacy, D. B.**, **Wu, Z.**, **Finkelstein, A.** et al., A phenylalanine clamp catalyzes protein translocation through the anthrax toxin pore. *Science* 2005. **309**: 777–781.

45 **Sacks, D. L.** and **Melby, P. C.**, Animal models for the analysis of immune responses to leishmaniasis. *Curr. Protoc. Immunol.* 2015. **108**. https://doi.org/10.1002/0471142735.im1902s28

46 **Cossarizza, A.**, **Chang, H. D.**, **Radbruch, A.**, **Acs, A.**, **Adam, D.**, **Adam-Klages, S.**, **Agace, W. W.** et al., Guidelines for the use of flow cytometry and cell sorting in immunological studies (second edition). *Eur. J. Immunol* 2019. **49**: 1457–1973.

Abbreviations: **AAM**: alternatively activated macrophage · **AM**: alveolar macrophages · **BMDMs**: BM-derived macrophages · **DFO**: deferoxamine · **dLN**: draining lymph node · **DPTA-NONOate**: dipropylenetriamine NONOate · **ETC**: electron transport chain · **LPM**: large peritoneal macrophages · **PEL**: peritoneal lavage · ***Ptgs2***: prostaglandin-endoperoxide synthase 2 · **RFP**: red fluorescence protein · **SPM**: small peritoneal macrophages

Full correspondence:: Prof. Manfred Kopf, ETH Zürich, Otto-Stern-Weg 7, 8093 Zürich, Switzerland
e-mail: Manfred.Kopf@ethz.ch

Received: 6/12/2020
Revised: 2/6/2021
Accepted: 8/7/2021
Accepted article online: 19/7/2021